


Visualizing reaction pathway for the photo-transformation of NO₂ and N₂ into NO over WO₃ photocatalyst

Joseph Che-Chin Yu¹ · Janusz Lasek² · Van-Huy Nguyen³ · Yi-Hui Yu¹ · Jeffrey C. S. Wu¹ 

Received: 16 May 2017 / Accepted: 7 July 2017
© Springer Science+Business Media B.V. 2017

Abstract A photo-transformation of NO₂ into NO at the N₂ presence is discovered over a WO₃ photocatalyst under UV/visible light irradiation. During the photoreaction, we found that both NO₂ and N₂ disappear and additional NO appears at the same time. A reaction pathway is proposed and verified by the results of an online chemiluminescence NO_x analyzer, GC-TCD, and in situ DRIFT monitoring of the reactants and products in mixtures. The collected data indicates that $\text{NO}_2 + \frac{1}{2} \text{N}_2 \rightarrow 2\text{NO}$ is an overall reaction of this photocatalytic reaction over a WO₃ photocatalyst.

Electronic supplementary material The online version of this article (doi:[10.1007/s11164-017-3065-6](https://doi.org/10.1007/s11164-017-3065-6)) contains supplementary material, which is available to authorized users.

Joseph Che-Chin Yu and Janusz Lasek contributed equally to this article.

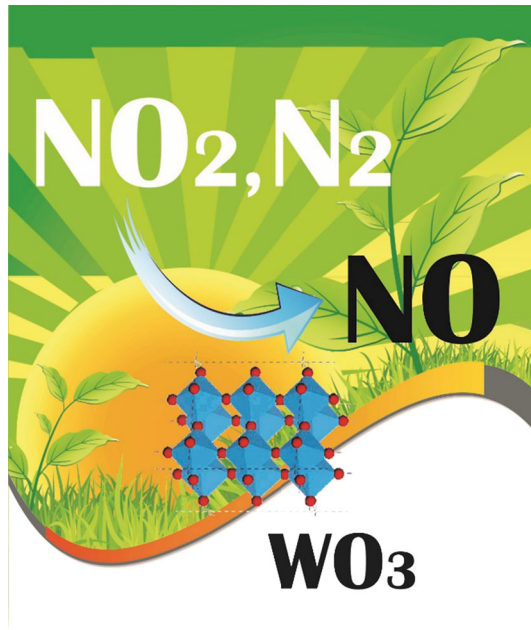
✉ Jeffrey C. S. Wu
cswu@ntu.edu.tw

¹ Department of Chemical Engineering, National Taiwan University, Taipei 10617, Taiwan

² Institute for Chemical Processing of Coal, ul. Zamkowa 1, 41-803 Zabrze, Poland

³ Faculty of Chemical and Environmental Engineering, Lac Hong University, No. 10 Huynh Van Nghe, Buu Long, Bien Hoa, Dong Nai, Vietnam

Graphical Abstract



Keywords Nitrogen dioxide (NO_2) · Nitrogen monoxide (NO) · Photocatalysis · Tungsten trioxide (WO_3) · Reaction pathway

Introduction

As we know, nitrogen monoxide (NO) and nitrogen dioxide (NO_2), which are considered together as nitrogen oxides (NO_x), have main effects on terrestrial and aquatic ecosystems. NO , which is majorly emitted from vehicle engines and industrial combustion process, causes air pollution and acid rain. However, NO could play a positive role in human health, such as in inhalation therapy (especially babies) [1, 2], an antimicrobial agent [3], a pharmaceutical drug [4], and compounds for food treatment [5]. It is worth mentioning that NO could easily be transformed to one of the most dangerous air pollutants, NO_2 , which plays a major role in acid rain and the formation of ozone. Moreover, prolonged exposure to NO_2 might cause inflammation of lung tissue, bronchiolitis fibrosa obliterans, and silo-filler's disease, and increased incidence of acute respiratory illness in children [6, 7].

Playing an important role in human and ecosystems, the NO_x topic has received a lot of attention, such as the abatement of NO_x emissions [8–11], and a NO_x sensor [7, 12–14]. It is noteworthy that many of these NO_x studies were carried out at high temperature, while there is a limit study on photocatalysis that could be operated at low temperature, resulting in a comparatively low cost, efficiency, and convenience.

Among feasible candidates for UV/visible light photocatalysts, tungsten oxide (WO_3) has attracted considerable interest for various potential applications due to its promising physical and chemical properties [15]. It has a very efficient photocatalyst for water splitting [16], and also is often applied as a component for making NO_x sensors [17–20].

In this study, a new photocatalytic reaction to transform NO_2 and N_2 into NO over WO_3 catalyst was successfully discovered. In addition to the UV-light, artificial sunlight from a solar simulator with an Air Mass 1.5 Global (AM1.5G) filter was also used to drive this photo-transformation. A reaction pathway was proposed to gain new insights into the transformation of NO_2 and N_2 into NO by combining an online chemiluminescence NO_x analyzer, GC-TCD, and in situ DRIFT. The online chemiluminescence NO_x analyzer and GC-TCD are used to analyze the reaction products from the continuous flow and batch photoreactors, respectively. The in situ DRIFT is used to observe the changes of surface-adsorbed species during the reactions. The results provide direct evidence that both NO_2 and N_2 participate in the photocatalytic reaction to generate NO over WO_3 photocatalyst.

Experimental

Characterization of photocatalyst

Tungsten oxide (WO_3 , CAS No. 1314-35-8, powder, 99.995%) photocatalyst was purchased from Sigma-Aldrich Corporation. An X-ray diffractometer (XRD, Ultima IV, Rigaku, Tokyo, Japan) equipped with $\text{Cu K}\alpha$ (1.5418 Å) was used to verify the crystalline structure of the photocatalyst. The UV–Vis diffuse reflectance spectrum of the photocatalyst was fully recorded over the range 300–600 nm by a Cary 100 UV-visible spectrometer (UV–Vis, Varian Cary 100, Agilent Technologies, Santa Clara, CA, USA). BaSO_4 was used as the reflectance standard.

Continuous flow photoreactor

The photocatalytic reaction was evaluated in a continuous flow system by using a plate-shape photoreactor (alumina alloy 6061, 0.15 mL). The scheme of the photoreactor is shown in Fig. 1a. Typically, 0.1 g photocatalyst was uniformly spread on the photoreactor irradiated by either a 200 W mercury arc lamp (Exfo S1500) or a 300 W xenon lamp (Newport, USA). The light intensity of the Hg arc lamp, which was measured at the quartz window of the photoreactor by using a GOLDILUX radiometer/photometer (UV-A Probe/UV-C Probe), was 200 mW cm^{-2} . A 300 W Xe lamp was used with an AM1.5G filter to simulate the sunlight that has the same power and spectral distribution of the sun at a 48.5° zenith angle. The influx was approximately 97 mW cm^{-2} . A gas mixture (Air product, Ltd) was composed of 40 ppm NO_2 , 1000 ppm NO and N_2 for balance (>99.9%) with a flow rate of 10 ml min^{-1} . Before the irradiation started, the feed was purged into the photoreactor for 8 h to remove the air in the pipeline and

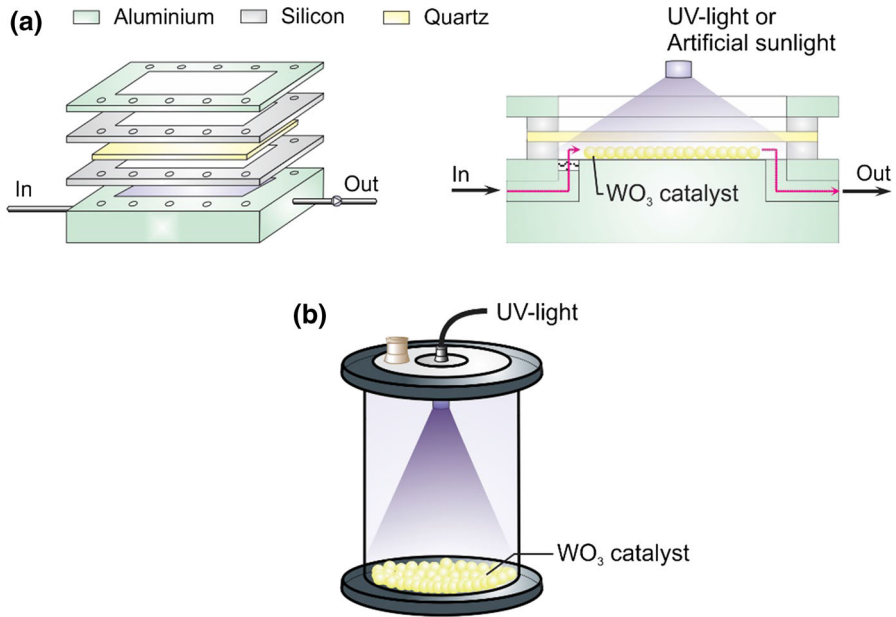


Fig. 1 The scheme of photoreactors: **a** the continuous flow photoreactor and **b** the batch photoreactor

photoreactor. The NO and NO₂ concentrations were measured by the online chemiluminescence NO_x analyzer (Teledyne Instruments, M200E).

Batch photoreactor

The photocatalytic reaction was conducted on a batch system using the cylindrical photoreactor (385 mL), which is shown in Fig. 1b. Firstly, 0.1 g WO₃ photocatalyst was packed in the bottom of the photoreactor. The 200 W Hg UV lamp (Exfo S1500), which had its light intensity adjusted to 48 mW cm⁻², was guided by an optical fiber that could be inserted into the photoreactor. To precisely measure the changes of NO and N₂, the gas mixture (with He as a balancing gas) was used for this experiment. The feed (Air product, Ltd) was composed of 250 ppm N₂, 750 ppm NO₂ and He for balance with the total pressure of 1.50 bar. The gas composition was analyzed by a GC-TCD (Young Lin Ltd.) equipped with two packed columns for the separation of N₂, NO, and NO₂ (Hayesep D 100/120 mesh, and Porapak Q). Before the irradiation, the photoreactor was purged by the feed for 8 h to remove the air in the pipeline and photoreactor. Then, three data points were sampled (at -60, -30, 0 min), before the UV-light was turned on (at 0 min). After the irradiation had started, data points were sampled at 3, 30, 60, 120, and 180 min, respectively.

In-situ DRIFT analysis

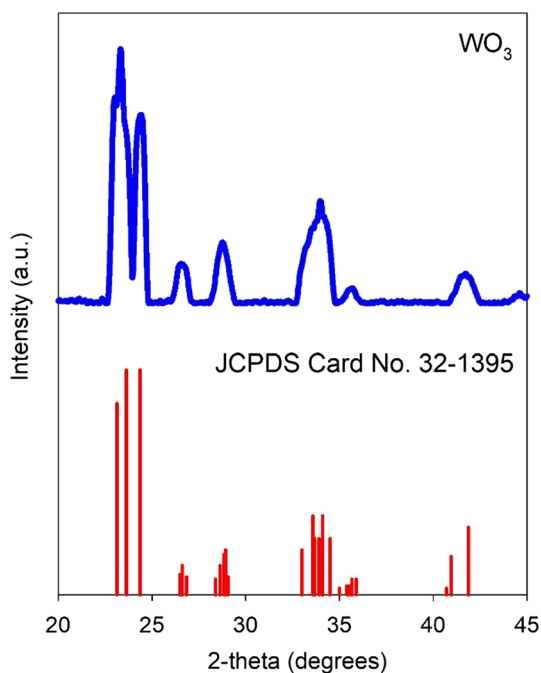
The photocatalytic reaction was studied by diffuse reflectance infrared Fourier transform (DRIFT) spectroscopy under UV-light irradiation (Exfo S1500, 200 mW cm^{-2}). A 316 stainless-steel dome photoreactor (Harrick HVC-DRP-1) was used with three windows, including two KBr windows transparent to both IR and UV-light for IR transmittance and a quartz window transparent to UV-light, but slightly transparent to IR light for UV irradiation [21]. All the gases were passed through a moisture-trap before entering the photoreactor to reduce water interference. The scanning range of IR was $650\text{--}4000 \text{ cm}^{-1}$ with a resolution of 4 cm^{-1} using a mercury-cadmium-telluride (MCT) detector in a Nexus 470 IR spectrometer (Thermo Nicolet), and each IR spectrum was obtained by 32 scans. Before the irradiation, the photocatalyst was placed in the photoreactor and purged by He for 8 h to remove the air in the pipeline and the photoreactor. Next, the mixture of 40 ppm NO_2 , 1000 ppm NO and N_2 for balance was introduced for 8 h not only to remove the air but also make the adsorption/desorption process on the photocatalyst surface steady. Lastly, the UV-light was turned on (at 0 min) and recorded at 1, 2, 3, 5, 10 and 30 min.

Results and discussion

Characterization of photocatalyst

Figure 2 displays the X-ray diffraction (XRD) pattern of the commercial WO_3 photocatalyst. All the peaks on the spectrum have crystalline features consistent

Fig. 2 X-ray diffraction patterns of WO_3 photocatalyst and its reference (JCPDS card No. 32-1395)



with WO_3 crystal (JCPDS No. 32-1395). The diffraction pattern of WO_3 powder has a peak centered at $2\theta = 23.6^\circ, 24.4^\circ, 23.1^\circ, 34.1^\circ, 33.6^\circ, 41.9^\circ$ corresponding to the (020), (200) (002), (202), (-202) , (222). Figure 3 shows the UV–Vis spectra of the WO_3 photocatalyst. Clearly, the photocatalyst has an absorption range of 300–460 nm including visible-light wavelength, and the calculated bandgap was 2.70 eV.

Continuous flow photoreactor for detection of NO_2 elimination and NO formation

Figure 4 shows a specific rate of NO_2 transformation into NO monitored by an online chemiluminescence NO_x analyzer. The formation of NO and elimination of NO_2 were observed simultaneously under UV-light irradiation in Fig. 4a, and the average molar ratio of NO/NO_2 within 7 h equaled 2.19 in a steady state. Furthermore, the experiment was also conducted under visible-light irradiation as shown in Fig. 4b. Because of the nature of WO_3 itself, visible-light could be easily adsorbed by the WO_3 photocatalyst, which could be proved by Fig. 3. Moreover, the average molar ratio of NO/NO_2 within 5 h equaled 2.12 in a steady state. The NO/NO_2 ratio was calculated by Eq. (1):

$$\text{ratio} = \frac{|\text{NO}_{(D)} - \text{NO}_{(L)}|}{|\text{NO}_{2(D)} - \text{NO}_{2(L)}|}, \quad (1)$$

where $\text{NO}_{(D)}$, $\text{NO}_{2(D)}$ —an average molar fraction of NO or NO_2 before irradiation; $\text{NO}_{(L)}$, $\text{NO}_{2(L)}$ —a molar fraction of NO or NO_2 during the photocatalytic reaction. According to this observation and the confirmed knowledge, a mechanism of photo-transformation of NO_2 into NO over WO_3 photocatalyst was proposed.

In the beginning, electrons and holes were generated by the light irradiation, and these active sites could be created at the WO_3 surface [22]. This typical behavior of

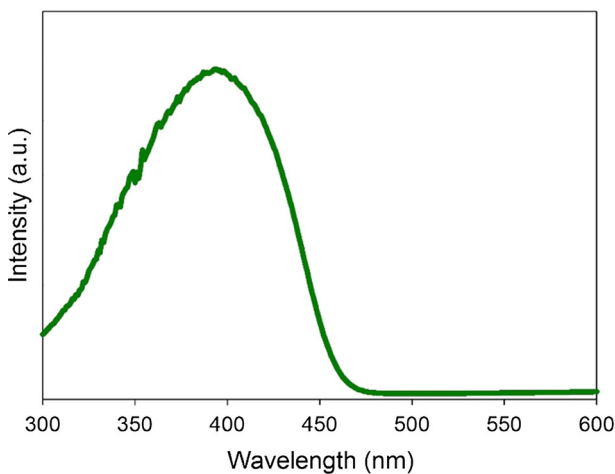


Fig. 3 UV–Vis absorption of WO_3 photocatalyst

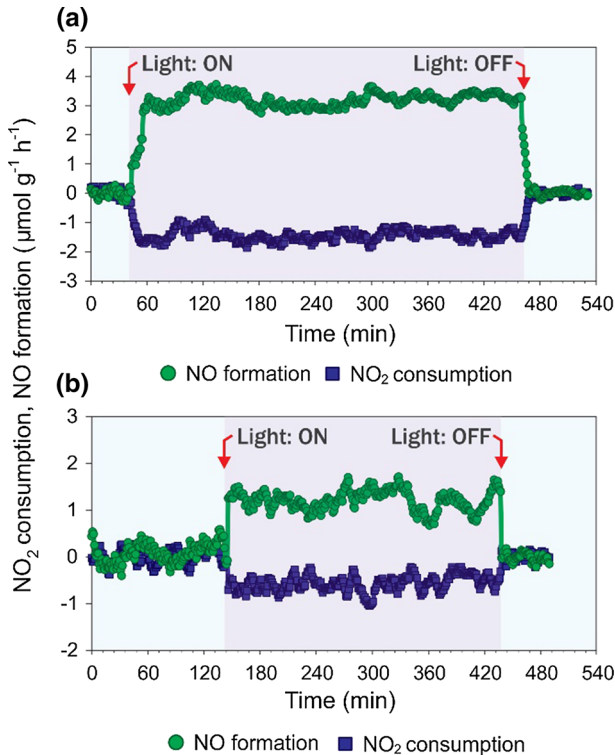


Fig. 4 The NO₂ consumption, NO formation rate over WO₃ under **a** UV-light **b** artificial sunlight irradiation. Conditions: NO: 1000 ppmv, NO₂: 40 ppmv, N₂: balance; total flow 10.0 ± 0.1 ml/min, at room temperature

photocatalysts is shown in Eq. (2). Next, Eq. (3) related to the photocatalytic reaction that occurred at the WO₃ surface was proposed because WO₃ photocatalyst not only has been proven as a sensor, but its sensitivity to NO₂ has been much higher than NO [17, 23]. This phenomenon was observed by measuring the gradually decreasing conductivity of WO₃ because the additional electrons came from the conduction band of WO₃ [18, 24]. Furthermore, the active complex, WO₄^{*}, was generated by the combination of O_{ads}⁻ and WO₃⁺ as shown in Eq. (4). WO₄^{*} represents an active complex created during light irradiation, and the creation of the active complex was proposed in many photocatalytic reactions using Ti, V, Cr, Mo... oxide photocatalysts among photo-deNO_x processes [25]. These charge-transfer photo-excited complexes of these metal oxides had high reactivity due to their efficient interaction of the complexes and reactant molecules. The Eqs. (2–4) are comprehensible, and they are consistent with the NO formation observed by a chemiluminescence NO_x analyzer.





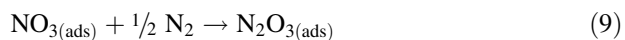
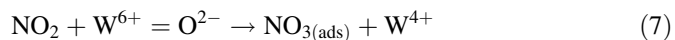
However, although the detected NO formation and NO₂ elimination could be explained by the Eqs. (2–4), the observation that the NO/NO₂ ratio roughly equaled to 2 (2.19 and 2.12 in UV-light and visible-light irradiation, respectively) has not been resolved. Thus, Eq. (5) was proposed, showing that the active complex, WO₄^{*}, could react with N₂ to form the NO. Since there was only N₂, NO, and NO₂ in the continuous flow photoreactor, using N₂, which was abundant in the photoreactor (>99.9%), to reduce NO₂ seemed to be the only reaction pathway.



Lastly, the Eqs. (2–5) could form a cycle and WO₃ photocatalyst was unchanged. These equations were summarized by the overall reaction as shown in Eq. (6), and it agreed with the observed molar NO/NO₂ ratio, which was equal to near two.

In-situ DRIFT analysis

Figure 5 shows the in situ DRIFT results in the Harrick photoreactor. The spectra were obtained at 1, 2, 3, 5, 10 and 30 min after the UV-light was turned on, respectively. Neither W⁵⁺–NO nitrosyls with ν(NO) stretching vibrations at 1843–1856 cm⁻¹ nor W⁴⁺(NO)₂ dinitrosyls with the band at 1691–1700 cm⁻¹ was observed in the spectra under the UV-light irradiation, indicating that WO₃ did not form any metal nitrosyl complexes with the exposure of NO, NO₂ and N₂ mixture for 8 h [26–28]. Moreover, NO can be recognized in the region 2080–1880 cm⁻¹ and the region 1680–1600 cm⁻¹ can be ascribed to NO₂ [29]. The most important observation of these spectra was that NO₂ gradually disappeared (negative peak 1623 cm⁻¹) and NO appeared (peak 1960 cm⁻¹) simultaneously during the photocatalytic reaction. Additionally, N₂O₃ could be observed in regions 1500–1530 cm⁻¹, and 1300–1330 cm⁻¹ [30, 31]. These peaks were not as significant as NO and NO₂ because N₂O₃ might be an intermediate adsorbed on the photocatalyst, then it could further undergo self-ionization to the NO⁺ and NO₂⁻ [32]. To sum up, Eqs. (7–10) were proposed as a simplified mechanism according to the literature [29, 31, 32] and these experimental observations.



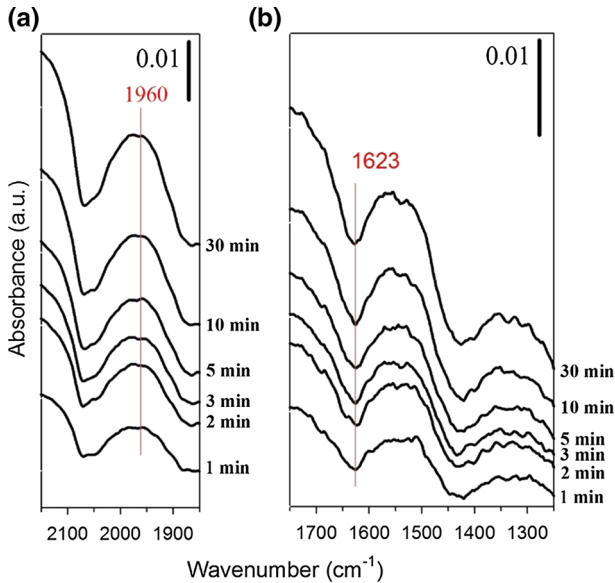
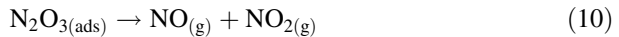


Fig. 5 The in situ DRIFT spectra of NO_2 transformation photocatalytic reaction under UV-light irradiation: **a** NO formation, **b** NO_2 elimination and N_2O_3 formation



The mechanism was simplified because adsorption and desorption processes were omitted. Additionally, note that the Eq. (11) is known as a self-ionization reaction [29]:



However, in the case of a photocatalytic reaction, it was reasonable that both of NO and NO_2 were created by electrons and holes, which are always present in the photocatalytic reaction during the UV-light irradiation, respectively. Moreover, when Eqs. (7–10) were summarized; the overall reaction was the same as Eq. (6) that could also explain why the NO/ NO_2 ratio equaled two.

Batch photoreactor for detection of NO formation and N_2 elimination

In the previous section, the Eqs. (5–6) have not been explained well because neither the chemiluminescence NO_x analyzer nor the IR instrument could detect the N_2 concentration. To testify that N_2 would participate in the photocatalytic reaction, the batch system introduced a NO_2 and N_2 mixture balance with He (>99.8%) that was used to precisely measure the changes of NO and N_2 concentration varying with time.

Figure 6 shows the time profile of both N_2 and NO concentration. The UV-light was turned on at 0 min. Before the irradiation started, the composition of gas

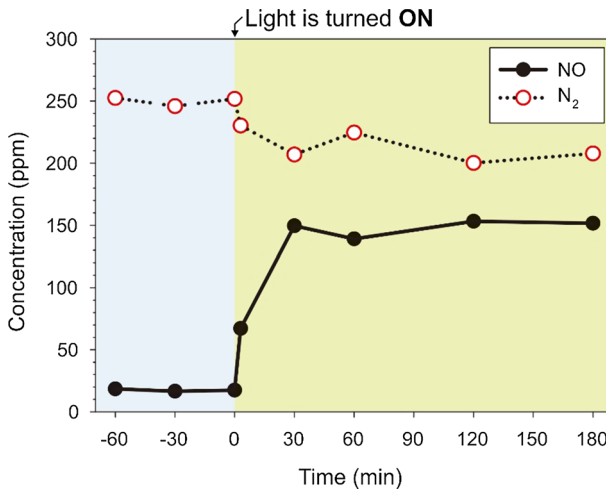


Fig. 6 Reaction time profile for the photocatalytic reaction of NO and N₂ in the batch photoreactor under UV-light irradiation. Conditions: N₂: 250 ppm, NO₂: 750 ppm; Total pressure: 1.50 bar

mixture remained stable at -60 , -30 and 0 min, showing that the adsorption and desorption were in dynamic equilibrium. After the UV-light had been turned on, the NO concentration increased while N₂ concentration decreased right after the irradiation for 3 min. Thus, Eq. (5) was plausible because the N₂ participated in the photocatalytic reaction. Then, the photocatalytic reaction became thermodynamically stable at 30 min, that is, the batch system was in the steady state. In addition, more data points in the steady state were acquired at 60, 120 and 180 min, respectively, and they could be used for the further calculation. The NO/N₂ ratio was calculated by Eq. (12):

$$\text{ratio} = \frac{|\text{NO}_{(D)} - \text{NO}_{(L)}|}{|\text{N}_{2(D)} - \text{N}_{2(L)}|}. \quad (12)$$

The NO/N₂ ratio computed in the steady state (at 30, 60, 120, and 180 min) equaled 3.26. This value was close to the stoichiometry of Eq. (6) that demonstrates the formation of NO should be four times as high as the elimination of N₂. This result could explain the overall reaction that was suitably described with Eq. (6).

Conclusions

In brief, a new photocatalytic reaction to transform NO₂ and N₂ into NO was successfully discovered over WO₃ photocatalyst. In addition to the UV-light, artificial sunlight also showed a good photocatalytic performance. An insight into the reaction pathway of reaction has been revealed. The overall reaction, $\text{NO}_2 + \frac{1}{2} \text{N}_2 \rightarrow 2\text{NO}$, was proposed based on the observed species presenting during the

experiment, which was verified by a chemiluminescence NO_x analyzer, GC-TCD, and in situ DRIFT.

Acknowledgements The research was investigated under the bilateral Taiwanese-Polish Joint Research Project. The authors gratefully acknowledge the financial support by the Ministry of Science and Technology, Taiwan, under Grant NSC 103-2923-E-002-002-MY3, and National Centre for Research and Development, Poland, Agreement No. DKO/PL-TW1/2/2013.

References

1. I. George, S. Xydas, V.K. Topkara, C. Ferdinando, E.C. Barnwell, L. Gableman, R.N. Sladen, Y. Naka, M.C. Oz, *Ann. Thorac. Surg.* **82**, 2161–2169 (2006)
2. F.L.M. Ricciardolo, P.J. Sterk, B. Gaston, G. Folkerts, *Physiol. Rev.* **84**, 731–765 (2004)
3. A. Ghaffari, C.C. Miller, B. McMullin, A. Ghahary, *Nitric Oxide* **14**, 21–29 (2006)
4. A.B. Shekhter, V.A. Serezhenkov, T.G. Rudenko, A.V. Pekshev, A.F. Vanin, *Nitric Oxide* **12**, 210–219 (2005)
5. D. Cornforth, in *Nitric Oxide*, ed. by L. Jack Jr. (Academic Press, San Diego, 1996), pp. 259–287
6. D. Zhang, Z. Liu, C. Li, T. Tang, X. Liu, S. Han, B. Lei, C. Zhou, *Nano Lett.* **4**, 1919–1924 (2004)
7. R. Kumar, O. Al-Dossary, G. Kumar, A. Umar, *Nano-Micro Lett.* **7**, 97–120 (2015)
8. Y. Sun, E. Zwolińska, A.G. Chmielewski, *Crit. Rev. Env. Sci. Technol.* **46**, 119–142 (2016)
9. V.I. Pârvulescu, P. Grange, B. Delmon, *Catal. Today* **46**, 233–316 (1998)
10. K. Skalska, J.S. Miller, S. Ledakowicz, *Sci. Total Environ.* **408**, 3976–3989 (2010)
11. J. Stein, in *Diesel Engine Management*, ed. by K. Reif (Springer, Wiesbaden, 2014), pp. 178–199
12. K. Satake, A. Katayama, H. Ohkoshi, T. Nakahara, T. Takeuchi, *Sens. Actuator B-Chem.* **20**, 111–117 (1994)
13. N. Yamazoe, N. Miura, *Sens. Actuator B-Chem.* **20**, 95–102 (1994)
14. T. Addabbo, F. Bertocci, A. Fort, M. Mugnaini, L. Shahin, V. Vignoli, S. Rocchi, R. Spinicci, M. Gregorkiewitz, in *Sensors: Proceedings of the Second National Conference on Sensors, Rome 19–21 February, 2014*, ed. by D. Compagnone, F. Baldini, C. Di Natale, G. Betta, P. Siciliano (Springer, Cham, 2015), pp. 211–215
15. S.H. Baeck, K.S. Choi, T.F. Jaramillo, G.D. Stucky, E.W. McFarland, *Adv. Mater.* **15**, 1269–1273 (2003)
16. H. Kato, M. Hori, R. Konta, Y. Shimodaira, A. Kudo, *Chem. Lett.* **33**, 1348–1349 (2004)
17. L. Chen, S.C. Tsang, *Sens. Actuator B-Chem.* **89**, 68–75 (2003)
18. H. Xia, Y. Wang, F. Kong, S. Wang, B. Zhu, X. Guo, J. Zhang, Y. Wang, S. Wu, *Sens. Actuator B-Chem.* **134**, 133–139 (2008)
19. T. Kida, A. Nishiyama, Z. Hua, K. Suematsu, M. Yuasa, K. Shimanoe, *Langmuir* **30**, 2571–2579 (2014)
20. X. An, J.C. Yu, Y. Wang, Y. Hu, X. Yu, G. Zhang, *J. Mater. Chem.* **22**, 8525–8531 (2012)
21. J.C.S. Wu, Y.-T. Cheng, *J. Catal.* **237**, 393–404 (2006)
22. G.R. Bamwenda, K. Sayama, H. Arakawa, *J. Photochem. Photobiol. A* **122**, 175–183 (1999)
23. G. Sberveglieri, L. Depero, S. Groppelli, P. Nelli, *Sens. Actuator B-Chem.* **26**, 89–92 (1995)
24. O.V. Safonova, G. Delabouglise, B. Chenevier, A.M. Gaskov, M. Labeau, *Mater. Sci. Eng. C* **21**, 105–111 (2002)
25. M. Anpo, T.-H. Kim, M. Matsuoka, *Catal. Today* **142**, 114–124 (2009)
26. Y. Yan, Q. Xin, S. Jiang, X. Guo, *J. Catal.* **131**, 234–242 (1991)
27. K. Hadjiivanov, P. Lukinskas, H. Knözinger, *Catal. Lett.* **82**, 73–77 (2002)
28. T. Weingand, S. Kuba, K. Hadjiivanov, H. Knözinger, *J. Catal.* **209**, 539–546 (2002)
29. M. Kantcheva, I. Cayirtepe, *J. Mol. Catal. A* **247**, 88–98 (2006)
30. M. Kantcheva, E.Z. Ciftlikli, *J. Phys. Chem. B* **106**, 3941–3949 (2002)
31. K.I. Hadjiivanov, *Catal. Rev.* **42**, 71–144 (2000)
32. E. Ito, Y.J. Mergler, B.E. Nieuwenhuys, H. van Bekkum, C.M. van den Bleek, *Micropor. Mater.* **4**, 455–465 (1995)